


Subgap states at ferromagnetic and spiral-ordered magnetic chains in two-dimensional superconductors. II. Topological classification

C. J. F. Carroll and B. Braunecker 

SUPA, School of Physics and Astronomy, University of St. Andrews, North Haugh, St. Andrews KY16 9SS, United Kingdom



(Received 12 August 2021; accepted 6 December 2021; published 22 December 2021)

We investigate the topological classification of the subgap bands induced in a two-dimensional superconductor by a densely packed chain of magnetic moments with ferromagnetic or spiral alignments. The wave functions for these bands are composites of Yu-Shiba-Rusinov-type states and magnetic scattering states and have a significant spatial extension away from the magnetic moments. We show that this spatial structure prohibits a straightforward extraction of a Hamiltonian useful for the topological classification. To address the latter correctly, we construct a family of spatially varying topological Hamiltonians for the subgap bands adapted for the broken translational symmetry caused by the chain. The spatial dependence in particular captures the transition to the topologically trivial bulk phase when moving away from the chain by showing how this, necessarily discontinuous, transition can be understood from an alignment of zeros with poles of Green's functions. Through the latter, the topological Hamiltonians reflect a characteristic found otherwise primarily in strongly interacting systems.

DOI: [10.1103/PhysRevB.104.245134](https://doi.org/10.1103/PhysRevB.104.245134)

I. INTRODUCTION

Until comparatively recently, the classification of physical phases relied primarily on the paradigm of spontaneously broken symmetries introduced by Landau. Over the last decades though, this scheme was complemented by the concept of topological phases. In the latter, the symmetries are preserved but locally similar states can have different global properties, associated for quantum systems typically with some twists in the wave functions that manifest themselves only when considering the full ensemble of eigenstates. The preservation of symmetries remains indeed a key feature of the topological phase classification as it is on the basis of the existence of symmetry protected, gapped states appearing on entrance to such phases [1]. Such protected states have resulted in a significant body of continually evolving research with broad and novel potential applications, including facilitating the possibility of topological quantum computing [2].

The universality of the symmetry concept allows quite broadly a characterization of the topological properties to be made in terms of effective Hamiltonians capturing the generic physics in the vicinity of points in the Brillouin zone that remain invariant under the specific symmetry operations. Topological phase transitions are characterized there by gap closures and reopenings, for instance by band inversion upon tuning of some control parameter. Most prominent is the invariance under time-reversal symmetry, and in combination with chiral and parity symmetry this has led to the topological classification table known as the tenfold way [3–6].

This type of classification is limited to no or weak interactions though, and strong interactions may lead to additional phases with intriguing properties. It is a matter of ongoing research to identify and classify such phases where a

broader toolkit is required beyond the symmetry classification of weakly interacting Hamiltonians [7–9]. One such tool is the classification based upon Green's functions [10–16], which is able to replicate the success of weakly interacting classifications, while allowing the possibility of more readily incorporating strongly interacting phases.

An interesting characteristic arising in a clear way from the Green's function based classification is that topological phase transitions can arise not only through gap closures at high symmetry points. A topological phase transition is bound to the generation of topological defects in some global property of the wave functions or the Hamiltonian when probed over the support of the system's spectrum. The appearance or vanishing of defects requires a singular behavior. This is conventionally expressed through the gap closing of the Hamiltonian, corresponding for the Green's functions to a merger of poles. But it is also possible in the absence of a gap closure by the merging of zeros of the Green's function [10,11], or the merging of a zero and a pole. As the latter is unlikely to occur in the absence of strong interactions, it is not ordinarily considered. Examples of this phenomenon are thus of significant fundamental interest to better understand the nature of topological phases broadly. One aspect of this paper is to reveal how such an example can be extracted from a weakly interacting system with a partially broken spatial translation symmetry. This results from the necessity of reconsidering how to obtain the topological classification in such a system, which comprises the other results of this paper.

Within this work, we build on the model and on key results developed in Ref. [17], henceforth called *Part I*, for the system shown in Fig. 1, i.e., a chain of densely packed magnetic scatterers embedded in a two-dimensional (2D) superconducting substrate. We show that the importance of the

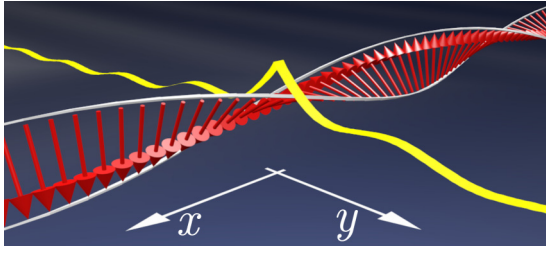


FIG. 1. Schematic representation of the continuous, spiral ordered line of magnetic moments at $y = 0$, periodic in π/k_m along the x direction. The yellow tape represents the modification of the local density of states and thus reflects the spatial extent of the subgap wave functions.

spatial structure of the subgap states over all wavelengths emphasized in Part I has a direct impact on the topological properties too, and we develop a transparent topological classification which accounts for the lack of translation symmetry. We indeed demonstrate that although the subgap states are confined near the interface and form one-dimensional (1D) bands, it is not straightforward to eliminate the transverse spatial degree of freedom to be able to use the established 1D topological classification methods. We, in fact, provide a rigorous proof based on Choi's theorem [18,19] that the often used convenient method of tracing out the transverse spatial degrees of freedom to obtain an effective 1D Hamiltonian is valid only for fully separable wave functions. This condition is met, for instance, for confined edge states of quantum Hall systems or topological insulators for which this elimination is thus applicable. It is, however, not met in the present case, and an uncritical application of such a method would lead to an incorrect topological classification.

To cure this problem, we make use of the full spatial information of the exact Green's function provided through Part I. The latter comprises, in particular, the long spatial extent of the wave functions created from scattering on the magnetic impurities, emphasized earlier for the long range of Yu-Shiba-Rusinov (YSR) states [20,21]. We introduce a family of spatially varying topological Hamiltonians that through the standard 1D classification methods provide at the impurity chain the correct topological invariants, but also incorporate the transition to the topologically trivial regions of the superconductor at large distances to the chain. By smoothly varying the distance from the chain, the thus obtained family of topological invariants displays novel exit and reentrance into a topologically nontrivial phase due to the interplay between poles and zeros of the underlying Green's function. This phenomenon occurs in a weakly interacting system and appears to be entirely due to geometric, interference-based considerations. This adds a property to the densely packed magnetic scatterers that is different to dilute chains of YSR states that can receive a more conventional 1D topological classification, which has been amply investigated in the literature [22–45], starting from the basic phenomenology of YSR states [46–48]. The importance put forward in Part I to determine the exact form of the Green's function of the superconductor with the magnetic impurity chain becomes essential here. Indeed, we show that only in the domains

where the often used long wavelength approximation (LWA) is applicable, the use of the conventional 1D classification methods followed from tracing out the spatial degrees of freedom remains valid. As the LWA is the extrapolation of tightly packed YSR states, this confirms the applicability of the used topological classification. But it also tells that another approach such as used here is necessary when the LWA no longer applies, which, as discussed in Part I, is in a topologically most interesting range of spiral magnetic order. Densely packed chains have been realized in experiment and show indeed a more complex band structure than expected from a simple YSR picture. For such systems, the proposed augmented classification method should be directly applicable.

The further structure of the paper is the following. In Sec. II, we summarize the model and the main result for the Green's function obtained in Part I. In Sec. III, we introduce the concept of topological Hamiltonians that will form the basis for the further discussion. In Sec. IV, we recall the essentials of the topological classification of the corresponding 1D system. Section V contains the core of this work, with the topological classification tailored to account for the 2D structure of the system. We conclude in Sec. VI. The analytical results are complemented by a numerical verification based on the tight-binding model already described in Part I. In the Appendix, we discuss the extension to the numerics for the topological classification.

II. MODEL AND GREEN'S FUNCTIONS

The model and its properties have been laid out in detail in Part I, and we therefore provide here only a high-level summary of its main features. We set $\hbar = 1$ throughout. The 2D superconductor is described by the Hamiltonian

$$H_0 = \sum_{\mathbf{k}, \sigma} \epsilon_{\mathbf{k}} c_{\mathbf{k}, \sigma}^\dagger c_{\mathbf{k}, \sigma} + (\Delta c_{-\mathbf{k}, \downarrow} c_{\mathbf{k}, \uparrow} + \text{H.c.}). \quad (1)$$

Here, $c_{\mathbf{k}, \sigma}$ are the electron operators for momenta $\mathbf{k} = (k_x, k_y)$ and spins $\sigma = \uparrow, \downarrow = +, -$. The dispersion $\epsilon_{\mathbf{k}} = (k_x^2 + k_y^2 - k_F^2)/2m$ has effective mass m and Fermi momentum k_F , and Δ is the s -wave bulk gap. Spatial coordinates are denoted by (x, y) . The dense chain of classical moments is placed at position $y = 0$ and runs along x . It scatters electrons through the Hamiltonian

$$H_m = V_m \int dx \mathbf{M}(x) \cdot \mathbf{S}(x, y = 0), \quad (2)$$

with scattering strength V_m , electron spin operator $\mathbf{S}(x, y)$, and the planar magnetic spiral formed by the classical spins, $\mathbf{M}(x) = \cos(2k_m x) \hat{\mathbf{e}}_1 + \sin(2k_m x) \hat{\mathbf{e}}_2$. In the latter expression, the parameter k_m expresses the spiral's periodicity of wavelength π/k_m , and $\hat{\mathbf{e}}_{1,2}$ are arbitrary orthogonal vectors. Although self-ordering mechanisms can lead to specific spiral periods [36,37,41–44,49–51], here we keep k_m as a free tuning parameter.

The k_x momentum transfer of $2k_m$ by scattering on H_m can be compensated by choosing the spin quantization axis perpendicular to $\hat{\mathbf{e}}_{1,2}$ and considering the gauge transformation, $c_{\mathbf{k}, \sigma} \rightarrow \tilde{c}_{\mathbf{k}, \sigma} = c_{(k_x - \sigma k_m, k_y), \sigma}$ [52]. In this new basis, $\mathbf{M}(x) \equiv \hat{\mathbf{e}}_1$ so that H_m corresponds to a ferromagnetic chain of scattering strength V_m applied perpendicular to the spin quantization

axis. As the transformation also shifts the dispersions $\epsilon_{\mathbf{k},\sigma} \rightarrow \epsilon_{(k_x+\sigma k_m, k_y)}$, the dispersions of the subgap bands created from scattering on H_m also depend sensitively on k_m , and indeed the spin-dependent shifts are equivalent to a uniaxial spin-orbit interaction [52].

In the gauge-transformed basis, translational symmetry along x is restored, and the problem is solved in a mixed momentum and real-space description in the variables (k_x, y) . Since H_m induces spin-flip scattering, an extended Nambu-spin basis is required, which we choose as

$$(\tilde{c}_{\mathbf{k},\uparrow}^\dagger, \tilde{c}_{\mathbf{k},\downarrow}^\dagger, \tilde{c}_{-\mathbf{k},\downarrow}, \tilde{c}_{-\mathbf{k},\uparrow}), \quad (3)$$

with the restriction $k_x \geq 0$ to avoid double counting of states. Notice that this basis is expressed in the gauge-transformed operators and does not have the minus sign that is used, e.g., in front of $\tilde{c}_{-\mathbf{k},\uparrow}$ in parts of the literature. The Pauli matrices acting in Nambu space will be denoted by τ_α and those acting in spin space by σ_α , for $\alpha = x, y, z$. We include, furthermore, with τ_0 and σ_0 , the corresponding unit matrices.

The system properties are characterized through the retarded Green's function in Nambu-spin space, which, for the full system, takes the form

$$G(\omega, k_x, y, y') = g(\omega, k_x, y - y') + g(\omega, k_x, y)T(\omega, k_x)g(\omega, k_x, -y'), \quad (4)$$

where the T matrix is given by the (ω_n, k_x) -dependent matrix,

$$T(\omega, k_x) = [(V_m \tau_z \sigma_x)^{-1} - g(\omega, k_x, 0)]^{-1}, \quad (5)$$

and $g(\omega, k_x, y)$ is the bulk Green's function in the absence of H_m . For the present model, the latter has the exact solution

$$g(\omega, k_x, y) = \sum_{\sigma} \frac{-i\pi\rho}{2k_F\sqrt{\tilde{\omega}^2 - \tilde{\Delta}^2 + i\eta}} \{ \tilde{\omega}_+ \xi_{\sigma} \tau_0^{\sigma} + \sigma \tilde{\Delta} \xi_{\sigma} \tau_x^{\sigma} + [(\kappa_{\sigma}^2 - 1)\xi_{\sigma} + \chi_{\sigma}] \tau_z^{\sigma} \}, \quad (6)$$

where $\rho = m/\pi$ is the 2D density of states at the Fermi energy, $\tilde{\omega} = \omega/E_F$ and $\tilde{\Delta} = \Delta/E_F$ are dimensionless frequency and gap, for $E_F = k_F^2/2m$, $\tau_{\alpha}^{\pm} = \tau_{\alpha}(\sigma_0 \pm \sigma_z)/2$, $\eta > 0$ is an infinitesimal shift, and $\tilde{\omega}_+ = \tilde{\omega} + i\eta$. Furthermore, we have defined

$$\kappa_{\sigma} = (k_x + \sigma k_m)/k_F, \quad (7)$$

$$\xi_{\sigma} = p_{\sigma,+}^{-1} e^{i|y|k_F p_{\sigma,+}} + p_{\sigma,-}^{-1} e^{-i|y|k_F p_{\sigma,-}}, \quad (8)$$

$$\chi_{\sigma} = p_{\sigma,+} e^{i|y|k_F p_{\sigma,+}} + p_{\sigma,-} e^{-i|y|k_F p_{\sigma,-}}, \quad (9)$$

with

$$p_{\sigma,\pm} = [1 - \kappa_{\sigma}^2 \pm (\tilde{\omega}^2 - \tilde{\Delta}^2 + i\eta)^{1/2}]^{1/2}. \quad (10)$$

In Part I, we provided a detailed analysis of the importance of using the Green's function of Eq. (6) and not any commonly used approximations. Equation (6) remains of fundamental importance in this paper, as any such approximation would lead to an incorrect topological classification.

The direct computation of G and T consists of a number of matrix multiplications and inversions and this last step is generally done numerically, though the relatively simple form allows for a number of analytic results, which we summarize in the following.

The poles of the Green's function provide the spectrum, and all subgap states arise from the poles of the T matrix; hence, $\det T^{-1} = 0$ at some $|\omega| < \Delta$ provides the criterion for the existence of a subgap state. The solution of $\det T^{-1}(\omega = 0, k_x = 0) = 0$ is of particular interest because it provides the condition for the interaction strength V_m at which the subgap states close the gap at the high symmetry point. One can analytically solve this equation for any spiral wave vector. If we define, with

$$C_m = \pi \rho V_m / k_F, \quad (11)$$

the dimensionless amplitude of the magnetic scattering strength, then the critical amplitude for the gap closure is given by

$$C_m^* = [(1 - k_m^2/k_F^2)^2 + \tilde{\Delta}^2]^{1/4}. \quad (12)$$

As discussed in Part I, the exact result of Eq. (12) bears a number of interesting features. The exponent of 1/4 rather than 1/2 as expected by comparison to a purely 1D model (see Sec. IV) occurs due to the dimensional mismatch between the substrate and the impurity chain. At a ferromagnetic interface with $k_m = 0$, the gap closing has only a weak dependence on $\tilde{\Delta}$ and can be interpreted as the result from the hybridization between the YSR states forming the Shiba bands. On the other hand, at $k_m = k_F$, one has $C_m = \tilde{\Delta}^{1/2}$, and thus a gap closure caused by the direct competition between magnetic scattering and pairing. This resembles a dimensionally renormalized Zeeman interaction, and as shown in Part I, indeed, YSR states and their hybridization are of no importance in this limit. We additionally point out that Eq. (12) is in excellent agreement with the self-consistent numerical solution of the lattice version of this problem, showing that Eq. (12) is indeed a general result and not specific to the chosen continuum model.

III. TOPOLOGICAL HAMILTONIANS

The topological classification of a material is based on the calculation of topological indices. Two types of approaches are common for bulk superconductors, based on either characteristics of the Hamiltonian at special points or integrals of Berry-type connections over the Brillouin zone. In the former category falls the common \mathbb{Z}_2 characterization determined from the sign of Pfaffians of matrices proportional to the Hamiltonian at time-reversal symmetric points in the Brillouin zone [53–56]. With such an approach, the classification of the purely 1D system of Sec. IV is immediate. The latter category refers to topological indices expressed, for example, through TKNN invariants, Chern numbers, and Zak phases [57,58]. These cases require the knowledge of the Bloch wave functions. Equivalent indices can be obtained through Green's functions [10,59] which has the advantage that interactions can be included as well [11–13,16]. Yet in their original formulations, these indices involve multiple products of Green's functions, their derivatives, and frequency integrals, in addition to momentum integrals. A large effort was therefore made to derive simpler equivalent expressions [12–15]. Notable is the replacement of the frequency ω integral by $\omega = 0$ and use of the Green's function then to define an effective topological Hamiltonian that correctly captures the topological classification [11,14,15,59–62]. The latter is

indeed rather intuitive since any Green's function is obtained through matrix elements of the resolvent $\hat{G}(\omega) = (\omega - H)^{-1}$ such that $H = -\hat{G}^{-1}(0)$. Subtleties arise since Green's functions are projections of the resolvent and their inversion does not reproduce the original (possibly interacting) Hamiltonian. But, notwithstanding the subtleties, they correctly capture the topological classification [14,15].

For a bulk system, the topological Hamiltonian can be defined through

$$H_{\text{bulk}}^{\text{top}}(\mathbf{k}) = -G_{\text{bulk}}^{-1}(\omega = 0, \mathbf{k}), \quad (13)$$

where G_{bulk} is the Green's function of the fully translationally symmetric system.

In the following, we will show that a similar approach can be adopted for our situation, although we have neither translational symmetry nor a periodic structure along the y situation. Despite this, we will demonstrate that a suitably adapted variant of Eq. (13) produces the correct topological classification if subtleties with the y dependence are appropriately taken into account.

IV. COMPARISON TO 1D SYSTEM

To obtain a baseline for the expected topological classification, we start by providing a brief account of the straightforward topological classification of a purely 1D model, along with the expected dimensional renormalization due to the embedding in a 2D system.

The 1D equivalent of Hamiltonian $H = H_0 + H_m$ [Eqs. (1) and (2)] is in the gauge-transformed basis

$$H(k_x) = \sum_{\sigma} \epsilon_{k_x + \sigma k_m} \tau_z^{\sigma} + \check{V}_m \tau_z \sigma_x + \Delta \tau_x \sigma_z, \quad (14)$$

written here not in second quantized form, but as a 4×4 matrix in Nambu-spin space at fixed k_x . We identify $\hat{\mathbf{e}}_1$ with the spin- x direction and $\tau_z^{\pm} = \tau_z(\sigma_0 \pm \sigma_z)/2$, and denote the magnetic potential \check{V}_m to avoid confusion with its counterpart in the 2D system. Since the \check{V}_m act on the entire system and not only on a line across the 2D system, they take the role of a uniform magnetic field whose original spiral was unwound through the gauge transformation. Equation (14) corresponds to the Hamiltonian of a ‘‘Majorana wire’’ [63–66], which has a known \mathbb{Z}_2 topological classification that can be obtained from the Pfaffians of the Hamiltonian at the time-reversal symmetric momenta [53].

Using this Hamiltonian, we calculate the topological invariant in the usual way by transforming $H(0)$ to a skew symmetric matrix $UH(0)$, where $U = \sigma_x \tau_x$ [taking this form because of the chosen Nambu-spin basis given by Eq. (3)], and by determining the sign of the Pfaffian $\text{pfaff}[UH(0)]$. The resulting phase diagram is plotted in Fig. 2 and shows the two distinct topological phases with the transition controlled by \check{V}_m . We should remark that for the continuum model, there is only one time-reversal symmetric momentum, $k_x = 0$, whereas in a lattice system, there would also be the momentum at the boundary of the Brillouin zone. In the latter, this second momentum is responsible for a reentrance to the topologically trivial phase at large magnetic interaction strength, which is absent in the present continuum model.

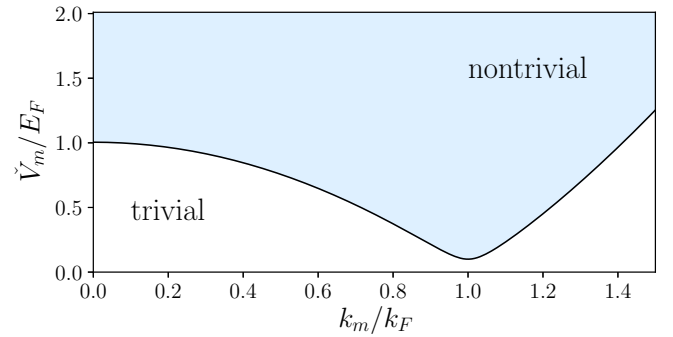


FIG. 2. Topological phase diagram for a pure 1D system with a spiral magnetic field, shown as a function of field winding momentum k_m vs field strength \check{V}_m , for $\Delta = 0.1E_F$. The white area is topologically trivial and the shaded area is nontrivial. The separating curve is described by Eq. (15). In this pure 1D case, the minimum at $k_m = k_F$ is reached at $\check{V}_m = \Delta$.

The boundary between two topologically distinct phases is characterized by a gap closure at a time-reversal invariant momentum. If we set $\check{C}_m = \check{V}_m/E_F$ in analogy to Eq. (11) and $\check{\Delta} = \Delta/E_F$, the gap closure at $k_x = 0$ for the 1D Hamiltonian requires an interaction strength $\check{C}_m = \check{C}_m^*$, with

$$\check{C}_m^* = \left[(1 - k_m^2/k_F^2)^2 + \check{\Delta}^2 \right]^{1/2}. \quad (15)$$

This critical amplitude has the same functional form as its 2D counterpart C^* given in Eq. (12), but with the exponent 1/2 instead of 1/4. This change is a dimensional renormalization, as mentioned above and explained further in Part I, due to the fact that in contrast to the 2D case, \check{V}_m acts on the full transverse extension of the wave functions. Besides this dimensional renormalization, the subgap states remain confined to the vicinity of the magnetic chain. We may thus expect that they retain a 1D character so that up to a renormalization of the phase boundaries, the phase diagram itself remains unchanged from the 1D case. As a motivational argument, we may indeed consider a procedure that continuously provides an increasing confinement transforming the 2D system into the pure 1D system. If this is done in each gapped phase in a manner such that the gap never closes, then the topological class of the subgap states should not change.

Such an argument alone, however, is naive as it neglects that in the 1D case, an extra confining potential is required, whereas in 2D, the confinement of the subgap states is controlled by Δ . In the transition between 1D and 2D, there is therefore a length scale at which the boundary condition for the confinement changes its physical origin. Since topology depends on global properties of the wave functions, a change of boundary condition must always be considered carefully, and we will see that indeed, the extension of wave functions across this scale is of importance. We therefore must consider in more detail the subtleties arising from the loss of translational symmetry or periodicity in the y direction.

V. LOCALIZED CLASSIFICATION

A. Absence of an effective 1D Hamiltonian

Due to the exponential confinement of the subgap wave functions to the region near the magnetic chain, the

electron motion is one dimensional. One may thus consider a description in terms of an effective 1D Hamiltonian, similar to those used for the 1D states appearing through confinement in heterostructures or to the edge bands in topological systems.

A complication arises here from the fact that the Nambu-spin and y degrees of freedom are highly mixed in the wave functions, as visible in Eqs. (6)–(10), whereas the conventional topological classification tools for 1D systems rely on the Nambu-spin structure alone. In the following sections, we provide a systematic discussion that in such a case, the topology of the subgap states can be reliably extracted by pinning y to the special value $y = 0$, followed by an exploration of the changes for $y \neq 0$.

In this section, however, we analyze the conditions under which the y coordinate can be traced out entirely, while maintaining the validity and convenience of the Nambu-spin based classification scheme. We formulate two conditions, (a) and (b) below, that a reduced Hamiltonian $H_{\text{eff}}^{\text{1D}}$ should fulfill and show that these conditions have a close connection with Choi's theorem on completely positive trace-preserving maps [18,19]. Based on this, we demonstrate that fulfillment of the conditions necessarily imposes a complete separability of the Nambu-spin and y degrees of freedom. This separability is generally not fulfilled in the present case and thus such an effective Hamiltonian cannot be constructed. A notable exception though is the regime in which the LWA is valid. For the latter, the necessary separability is approximately true, explaining why, for such a situation, a topological classification based on a simple tracing out of y provides correct results.

A dimensional reduction is an often tacitly used procedure in the study of low-dimensional systems. A quantum dot, for instance, is addressed commonly by operators creating and annihilating its different levels as entities without addressing the specific spatial structure. Interactions such as the Coulomb repulsion or spin orbit are effective integral quantities coupling the different levels. Such a description results from first analyzing the confinement of some noninteracting Hamiltonian, providing the set of basis functions for the confined geometry, and then expanding the full Hamiltonian in this basis. The eigenstates and the spectrum are then obtained by the diagonalization of the resulting Hamiltonian matrix, with the eigenstates given by an appropriate decomposition of the basis functions.

Our situation is distinct in that we already fully know the confined eigenstates. We have thus a different goal with the extraction of a lower-dimensional Hamiltonian. As explained above, our goal is to be able to work with the Nambu-spin based symmetries and topological classification methods without having to maintain the y dependence and, especially, without having to modify the methods.

The following proof when this is possible is not specific for the considered situation, but general for any type of Hamiltonian with a finite subset of discrete, localized states that are split off from the continuum.

For a fixed k_x , any full 2D Hamiltonian can formally be written as

$$H(k_x) = \sum_{n=1}^{N_n} \omega_n(k_x) |k_x, n\rangle \langle k_x, n| + \int d\alpha \epsilon_\alpha(k_x) |k_x, \alpha\rangle \langle k_x, \alpha|, \quad (16)$$

where n labels the N_n discrete subgap bands and α the continuum states. In our case with two subgap bands, we have $N_n = 2$, but we keep this number general, yet finite, for the following discussion.

The extraction of a 1D Hamiltonian requires two steps: the rather easy projection on subgap energies to remove the continuum states, and the elimination of the y coordinate.

In the following, we keep k_x as a fixed parameter and omit it from the notation, for simplicity, without loss of generality. The energy projection results in the Hamiltonian

$$H' = \sum_{n=1}^{N_n} \omega_n |n\rangle \langle n|. \quad (17)$$

The states $|n\rangle$ span an N_n -dimensional subspace \mathcal{H}' of the Hilbert space $\mathcal{H}_{N_s} \otimes \mathcal{H}_y$, where \mathcal{H}_{N_s} is the Nambu-spin space and \mathcal{H}_y is the space of square integrable functions of y .

We then seek a mapping Ω between operators on \mathcal{H}' and operators on \mathcal{H}_{N_s} such that $H_{\text{eff}}^{\text{1D}} = \Omega(H')$. We impose the following two conditions such a mapping needs to fulfill:

(a) The expectation values of any operator A on \mathcal{H}_{N_s} , acting with the identity on \mathcal{H}_y , must remain invariant. This means we impose

$$\langle n|A|n'\rangle = \text{Tr}\{|n'\rangle \langle n|A\rangle = \text{Tr}\{\Omega(|n'\rangle \langle n|)A\}. \quad (18)$$

Notice that A is kept outside the Ω mapping, which is not a physical requirement but the choice of convenience mentioned above.

(b) For each orthogonal projector $|n\rangle \langle n|$, the mapping produces again an orthogonal projector, $\Omega(|n\rangle \langle n|) = |u_n\rangle \langle u_n|$, with $|u_n\rangle$ in \mathcal{H}_{N_s} such that $\langle u_n|u_{n'}\rangle = \delta_{n,n'}$.

Condition (a) is the more stringent one, but condition (b) is the physical requirement as it ensures that $H_{\text{eff}}^{\text{1D}}$ remains a Hamiltonian on \mathcal{H}_{N_s} with a spectral decomposition and the same spectrum. An immediate necessary condition for (b) is that $N_n \leq \dim(\mathcal{H}_{N_s}) = 4$.

To evaluate the consequences of condition (a), let us choose a set of states $|\phi_p\rangle \in \mathcal{H}_y$, for $p = 1, \dots, N_p$, representing functions $\phi_p(y)$ such that

$$|n\rangle = \sum_{p=1}^{N_p} |v_n^p\rangle \otimes |\phi_p\rangle, \quad (19)$$

with $|v_n^p\rangle$ in \mathcal{H}_{N_s} . We assume that N_p is finite, and we see from Eqs. (6)–(10) that the $\phi_p(y)$ indeed are expressed by the small set of functions $\exp(\pm i|y|k_F p_{\sigma,\pm})$. Through an orthogonalization procedure such as the Gram-Schmidt method, we can choose the $|\phi_p\rangle$ to be orthonormal, $\langle \phi_p|\phi_{p'}\rangle = \delta_{p,p'}$. The normalization imposes, furthermore, that $\langle v_n^p|v_n^p\rangle = 1$, but otherwise there is no requirement for orthogonality on the $|v_n^p\rangle$. Equation (18) is then equal to

$$\langle n|A|n'\rangle = \sum_{p=1}^{N_p} \langle v_n^p|A|v_{n'}^p\rangle = \text{Tr}\left\{\sum_{p=1}^{N_p} |v_{n'}^p\rangle \langle v_n^p|A\right\}. \quad (20)$$

This relation must hold for any A and, consequently,

$$\Omega(|n'\rangle \langle n|) = \sum_{p=1}^{N_p} |v_{n'}^p\rangle \langle v_n^p| = \sum_{p=1}^{N_p} V_p |n'\rangle \langle n| V_p^\dagger. \quad (21)$$

The mapping Ω therefore takes the form of a Kraus decomposition [18,67], with the Kraus operators $V_p = \mathbb{1}_{N_s} \otimes \langle \phi_p |$, where $\mathbb{1}_{N_s}$ is the identity on Nambu-spin space. Noting that $\sum_p V_p^\dagger V_p$ produces the identity on \mathcal{H}' , we find that Ω falls in the remit of Choi's theorem [18], which states that any linear mapping from bounded operators acting on \mathcal{H}' to operators acting on \mathcal{H}_{N_s} that is completely positive and trace preserving is necessarily of the form of Eq. (21).

The minimum number N_p of necessary Kraus operators is known as the Choi rank, but otherwise the V_p can be freely chosen as long as they fulfill Eq. (21) and the identity condition on \mathcal{H}' .

We turn then to condition (b) and ask which choice of Kraus operators can guarantee the correct mapping of projectors, which thus has to take the form

$$\sum_{p=1}^{N_p} V_p |n\rangle \langle n| V_p^\dagger = \sum_{p=1}^{N_p} |v_n^p\rangle \langle v_n^p| = |u_n\rangle \langle u_n|. \quad (22)$$

Since $\dim(\mathcal{H}_{N_s}) = 4$, we can represent $|v_n^p\rangle$ as a $4 \times N_p$ matrix \mathcal{V}_n , and $|u_n\rangle$ as a length 4 column vector \mathcal{U}_n such that the latter equation becomes $\mathcal{V}_n \mathcal{V}_n^\dagger = \mathcal{U}_n \mathcal{U}_n^\dagger$. This means \mathcal{V}_n needs to be of rank 1, and therefore all its columns are directly linearly dependent. In this case, we have $|v_n^p\rangle = \lambda_n^p |u_n\rangle$, where the λ_n^p are numbers such that $\sum_{p=1}^{N_p} |\lambda_n^p|^2 = 1$. This, however, also imposes that

$$|n\rangle = |u_n\rangle \otimes \sum_{p=1}^{N_p} \lambda_n^p |\phi_p\rangle \equiv |u_n\rangle \otimes |\psi_n\rangle. \quad (23)$$

This result shows that conditions (a) and (b) are only compatible if the states $|n\rangle$ are separable in the sense of Eq. (23) in that for each n , the y dependence is in a single function $\psi_n(y) = \langle y | \psi_n \rangle$ multiplying the Nambu-spin states $|u_n\rangle$. The $|u_n\rangle$ must be orthogonal, but there is no orthogonality condition on the $|\psi_n\rangle$, only normalization as $\langle \psi_n | \psi_n \rangle = 1$. Note that Eq. (23) does not imply that the Choi rank is $N_p = 1$ as the $|\psi_n\rangle$ can be different for different n .

For separable $|n\rangle$, the mapping Ω becomes then particularly simple and results in just tracing out of the y degrees of freedom,

$$\begin{aligned} H_{\text{eff}}^{\text{1D}} &= \text{Tr}_y \{H'\} = \int dy \langle y | H' | y \rangle \\ &= \sum_{n=1}^{N_n} \omega_n |u_n\rangle \langle u_n| \int dy |\langle y | \psi_n \rangle|^2 = \sum_{n=1}^{N_n} \omega_n |u_n\rangle \langle u_n|. \end{aligned} \quad (24)$$

This result is remarkable in the sense that it confirms that for separable wave functions, the elimination of the confining degree of freedom by the intuitive simple integration is indeed the *only* way that does not change the physics of the other degrees of freedom. Separability is also encountered often for wave functions confined by some potential such as created by a heterostructure, or of edge states in quantum Hall systems, topological insulators, or topological superconductors, in which the envelope does not depend on spin, and in which further spatially dependent interactions that can hybridize the states are absent or negligible. In such a case, it is straightforward to integrate out the spatial dependence and obtain an

effective lower-dimensional Hamiltonian for the bound states only.

On the other hand, if the states are not separable, a Hamiltonian $H_{\text{eff}}^{\text{1D}}$ satisfying both conditions (a) and (b) cannot be constructed. This is indeed the general case for the subgap states at the magnetic chain. As mentioned before, this is seen from Eqs. (6)–(10) through the amplitudes ξ_σ and χ_σ , and their dependence on $p_{\sigma,\pm}$. For $|\omega| < 0$, the latter satisfy $p_{\sigma,+} = p_{\sigma,-}^*$. If we thus let $p_{\sigma,\pm} = p_\sigma \exp(\pm i\varphi)$ for $p_\sigma = |p_{\sigma,+}|$ and $\varphi = \pm \arg(p_{\sigma,\pm})$, we see that

$$\xi_\sigma = 2p_\sigma^{-1} \cos[yk_F p_\sigma \cos(\varphi) - \varphi] e^{-|y|k_F p_\sigma \sin(\varphi)}, \quad (25)$$

$$\chi_\sigma = 2p_\sigma \cos[yk_F p_\sigma \cos(\varphi) + \varphi] e^{-|y|k_F p_\sigma \sin(\varphi)}. \quad (26)$$

As long as $p_{\sigma,\pm}$ is complex, the division and multiplication by $p_{\sigma,\pm}$ adds opposite phase offsets $\pm\varphi$ to the y -dependent oscillations of ξ_σ and χ_σ , so that the y dependence is not globally factorizable from the different terms of the wave function, thus violating the separability of the wave function. The imaginary part of $p_{\sigma,\pm}$ is furthermore required for the exponential confinement and exists whenever $|\omega| < \Delta$.

To substantiate that indeed these factors of the Green's functions provide the relevant amplitudes of the wave function, let us note that we can write

$$\langle y | k_x, n \rangle \langle k_x, n | y' \rangle = \oint_{C_{k_x}} \frac{d\omega}{2\pi i} G(\omega, k_x, y, y'), \quad (27)$$

where C_{k_x} is a positively oriented closed contour encircling only the isolated pole $\omega_n(k_x)$ of the Green's function. Since at $|\omega| < \Delta$ the pole arises from the T matrix, we have

$$\begin{aligned} \langle y | k_x, n \rangle \langle k_x, n | y' \rangle &= g[\omega_n(k_x), k_x, y] \text{Res}T[\omega_n(k_x), k_x] \\ &\quad \times g[\omega_n(k_x), k_x, -y'], \end{aligned} \quad (28)$$

with $\text{Res}T$ the residue of the T matrix. Any y dependence is thus due to $g[\omega_n(k_x), k_x, y]$ and any y' dependence to $g[\omega_n(k_x), k_x, -y']$. Hence, the Green's functions g directly define the y dependence of the wave function, containing the exponential envelopes and the oscillations. As they are not separable in the sense above, the subgap states do not allow the reduction to an effective 1D Hamiltonian.

We should stress, however, that the lack of separability requires that the effect of the difference between the $p_{\sigma,\pm}$ is notable, and situations can exist in which approximate separability and thus an approximately valid 1D Hamiltonian can be obtained. Such a situation occurs when the exponential decay is fast compared with the oscillation period, expressed by the condition $\text{Im}p_{\sigma,+} \gg \text{Re}p_{\sigma,+}$. From Eq. (10), we see though that in the topologically most interesting limit of $\omega \rightarrow 0$, this condition does not hold. We then instead must consider the situation in which the phase shift φ making the oscillations of ξ_σ and χ_σ distinct is negligible. Since the characteristic range over which y is evaluated is set by the decay length $1/k_F p_\sigma \sin(\varphi)$, we see from Eqs. (25) and (26) that the phase difference $\pm\varphi$ can be neglected when $\cot(\varphi) \pm \varphi \approx \cot(\varphi)$, which is the case when $\cot(\varphi) \gg 1$. This represents thus the limit $\text{Im}p_{\sigma,+} \ll \text{Re}p_{\sigma,+}$, which is precisely the limit in which the long wavelength approximation (LWA) is applicable (see Part I). Full separability is then still not guaranteed as long as $p_{\sigma,\pm}$ have different spin σ dependence. But at the

topologically most significant $k_x = 0$, this spin dependence drops out and an approximate 1D Hamiltonian can be obtained by integrating out the y dependence. This property confirms why this method of obtaining such a Hamiltonian produces valid results in the LWA limit.

On the other hand, as discussed in depth in Part I, the range of applicability of the LWA becomes more and more restricted for increasing k_m and breaks down entirely at $k_m = k_F$, at which indeed $\text{Im}p_{\sigma,+} = \text{Re}p_{\sigma,+}$ for $k_x = 0$. For the topological classification of the subgap states, we therefore need a different approach, which we will describe next.

B. Dimensional embedding

Although it is not possible to obtain an effective 1D Hamiltonian, the wave functions remain 1D and we can expect that still some adjustment of the 1D topological classification schemes remains applicable. We thus aim to extract a 1D Hamiltonian solely for the purpose of the topological classification at the expense of removing any other physical significance. To this end, it is useful to examine the analogy of how 1D topological invariants arise as weak 2D topological indices in particular directions. For comparison, we consider the example provided in Ref. [68] through a generalized model of a $p + ip$ superconductor on a 2D square lattice. Instead of performing a full 2D analysis, in this paper, one of the momentum components k_x or k_y , is treated as a fixed parameter and tuned to a time-reversal invariant point. In terms of the other momentum, the Hamiltonian describes an effective 1D system, which in this case is equivalent to the Kitaev chain of a topological triplet superconductor. For the latter, the topological classification is determined in the standard 1D way, and the obtained topological indices are identified with the weak topological 1D indices of the 2D system. The combination of the weak indices provides the characterization of the full 2D system. The effective 1D Hamiltonians do not necessarily have any direct physical significance, but capture the topology at the significant time-reversal symmetric points. Since the system is translationally invariant, these points are labeled by the momenta k_x and k_y .

We are aiming for a similar extraction of an effective topological Hamiltonian. But due to the lack of translational symmetry along y , such a momentum space extraction of 1D Hamiltonians is not possible. To obtain the correct modification, let us recall the role of time-reversal symmetric points. In a fermionic system with time-reversal symmetry, each eigenstate has an orthogonal Kramers partner, i.e., its time-reversed counterpart of opposite momentum and equal energy. At a time-reversal symmetric point, the momenta of the Kramers partners coincide, but their orthogonality prevents them from hybridizing and lifting the energy degeneracy. Only if more than one Kramers pair is present is a hybridization possible between states not belonging to the same pair, and only in the presence of an even number of Kramers pairs can the degeneracy be lifted entirely. The parity of the number of Kramers pairs is expressed through the \mathbb{Z}_2 index associated with the time-reversal symmetric point, and the impossibility to hybridize defines a topologically nontrivial state. Although most of the considered 1D topological systems involve some magnetic elements breaking time reversal, there is throughout

either an emergent or an effective time-reversal symmetry [69] for the relevant states so that the \mathbb{Z}_2 classification remains a valid standard tool. A similar choice, yet without any justification of the used topological Hamiltonian, was applied for a tight-binding model at $y = 0$ in Ref. [70].

For the present case and in the limit of a large bulk gap Δ , the wave functions are in the y direction confined essentially to the magnetic chain position. The time invariant point is then given by $k_x = 0$ and, through the confinement, by $y = 0$. A classification through a topological Hamiltonian has to focus on this point. For a smaller Δ , the wave functions widen around $y = 0$, but any motion is still possible only in the x direction. The relevant time-reversal points remain k_x and y dependent. We notice that the operation of time reversal on the y dependence of the Green's function is to transform the latter as $G(y, y') \rightarrow G(y', y)$, and time-reversal invariance requires thus $y' = y$. This includes the chain center $y = y' = 0$, which will provide the primary criterion for the topological classification. But it further allows the characterization at $y = y' \neq 0$. As discussed in Sec. V A, we must not integrate out the y dependence, and instead below we will explore it further.

Consequently, we define the y -dependent family of topological Hamiltonians through [71]

$$H_{1D}^{\text{top}}(y) = -[G(\omega = 0, k_x = 0, y, y' = y)]^{-1}, \quad (29)$$

where $\omega = 0$, $k_x = 0$, and $y = y'$ are chosen to fulfill the necessary symmetry conditions of particle-hole symmetry at time-reversal invariant points in configuration space. The inverse is taken of the 4×4 matrix $G(0, 0, y, y)$.

The Hamiltonians $H_{1D}^{\text{top}}(y)$ represent a class of Hamiltonians obtained by slicing the 2D system into effective 1D segments at a distance y from the impurity chain. In this sense, they are similar to the effective 1D Kitaev-chain-type Hamiltonians used for the determination of the weak 1D indices in the bulk system, with y replacing the use of a momentum as parameter. But the y parameters are not limited to special values as time-reversal symmetry is built in through $y' = y$ in the Green's function, and y is tunable through all values. We will show that these Hamiltonians correctly produce the topological behavior of the subgap states in the vicinity of $y = 0$, reproducing the topological phase diagram of the pure 1D chain when taking into account the renormalized critical coupling strengths. The correctness of the Green's function at all wavelengths emphasized in Part I is of crucial importance here for the validity of the phase diagram, as could already be deduced from its significance on the nonseparability of the y -dependent wave function discussed in Sec. V A.

As the subgap bands are exponentially localized at the chain, the topology at large y must become trivial. Since the topological indices are integers, the passage to a trivial topology has to be abrupt and there must exist an effective boundary between the region near the chain and the rest of the superconductor. Through $H_{1D}^{\text{top}}(y)$, we can capture this behavior, but we should emphasize that $H_{1D}^{\text{top}}(y)$ is only to be taken as an archetypical representative of y -dependent topological Hamiltonians. The pure topological and not physical interpretation is furthermore underlined by noting that in addition to the symmetry considerations, the classification depends on the change of the sign of eigenvalues about the Fermi level and not

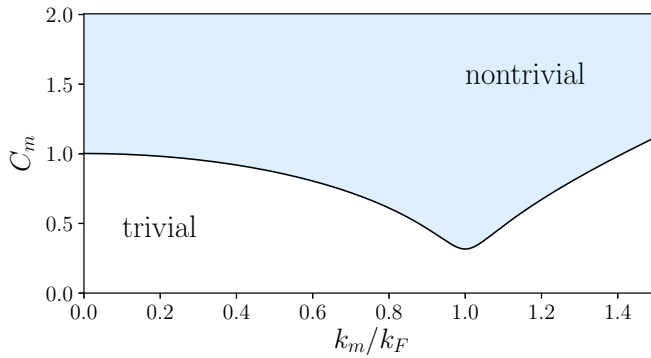


FIG. 3. Topological phase diagram obtained from the topological Hamiltonians $H_{1D}^{\text{top}}(y=0)$ as a function of spiral wave number k_m and magnetic scattering strength C_m , for $\tilde{\Delta} = 0.1$. This diagram corresponds to the phase diagram of the pure 1D model of Fig. 2, with the same color coding, upon the discussed dimensional renormalization, with values C_m^* [Eq. (12)] marking the transition by the solid line, instead of the values \check{C}_m^* [Eq. (15)]. Notably the transition at $k_m = k_F$ is now at the larger $C_m = \tilde{\Delta}^{1/2}$ instead of $C_m \propto \tilde{\Delta}$.

necessarily on the eigenvalues passing through the Fermi level [11–15,60,61]. Since the states do not change, the transition to the trivial phase with increasing y indeed cannot rely on Fermi level crossings and, as further investigated below, is instead bound to divergences in the spectrum of $H_{1D}^{\text{top}}(y)$ due to zeros in the defining Green's function, which themselves are the expressions of nodes in the subgap wave functions.

Before continuing, we should mention that alternative classification methods for spatially inhomogeneous systems were put forward several years ago in the form of local Chern markers [72], the Bott index [73], and noncommutative Chern numbers or Chern number densities [74–77]. Such quantities allow spatial variations in the topological classification. These approaches replace the derivatives in momentum space for the usual Chern numbers by traces over local coordinates in real space together with projections onto occupied states. We found though that for our current purpose, the method we propose is more readily accessible and provides the correct topological classification.

C. Topological classification near the chain

Since $H_{1D}^{\text{top}}(y)$ are matrices in Nambu-spin space, their topological classification is most easily done through the Pfaffians at time-reversal symmetric points, which for the continuum model is reduced to the behavior at $k_x = 0$ in the k_m shifted basis. The relevant topological index is then as in the 1D case above determined by the sign of $\text{pfaff}[UH_{1D}^{\text{top}}(y)]$ [56], where the matrix $U = \sigma_x \tau_x$ again transforms the Hamiltonian to a skew symmetric matrix. In Fig. 3, we plot the resulting topological phase diagram for the topological Hamiltonian at the position $y = 0$ of the impurity chain as a function of spiral winding k_m and dimensionless magnetic interaction strength C_m [see Eq. (11)]. The shaded areas are the topologically nontrivial range. In comparison with Fig. 2, we see that the results perfectly reflect the phase diagram of the pure 1D system under the aforementioned dimensional renormalization. The phase transition occurs when the subgap bands touch

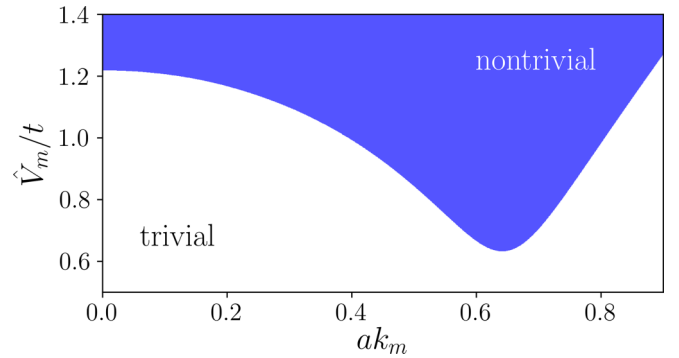


FIG. 4. Topological phase diagram obtained from the self-consistent numerical solution of the matching tight-binding model described in the Appendix, as a function of spiral wave number k_m and magnetic scattering strength \hat{V}_m . Scales are given in units of the hopping integral t and the lattice constant a . The pairing interaction and chemical potential are chosen to produce $\Delta \approx 0.1t$ and $k_F a \approx 0.65$. All the features of the analytic model are perfectly reproduced; only the numerical values of \hat{V}_m are not directly comparable with C_m because of the involved different density of states and effective mass.

at the Fermi level at $k_x = 0$. This is exactly at the critical interaction strength C_m^* given in Eq. (12), which replaces the \check{C}_m^* of the pure 1D system of Eq. (15). As there is no other gap closing at $k_x = 0$ and for the continuum model there is no finite momentum at the edge of the Brillouin zone, there is no mechanism for a phase transition at any other interaction strength.

To corroborate the validity of these results by an independent method, we compare them with the numerical solution of the tight-binding model that has already provided excellent quantitative verification in Part I. We perform two verifications, the first by comparing the matching topological invariants and the second by demonstrating the appearance of zero modes localized at the edges of a finite chain.

For the first verification, we also use the Pfaffians of the topological Hamiltonians for which we compute the Green's functions through their Lehmann representation from the eigenvalues and eigenvectors of the full 2D Hamiltonian. The Appendix contains a further description of the numerical evaluation. The numerical results are shown in Fig. 4, in which we again plot the diagram as function of k_m and the magnetic scattering strength, which we denote for the tight-binding model by \hat{V}_m . The agreement is excellent as the phases and the shape of the phase transition line are perfectly matched. However, we should note that the numerical values of \hat{V}_m for the transition are not the same because the densities of state of the two models are different. We remark furthermore that for the tight-binding model, we have only considered $k_x = 0$ and not its second time-reversal symmetric point $k_x = \pi/a$ at the edge of the Brillouin zone, as the latter is absent in the continuum model. We thus exclude in the tight-binding model the possibility to leave the topological phase at large C_m due to a gap closing at $k_x = \pi/a$.

The second verification of the validity of the topological classification through $H_{1D}^{\text{top}}(y=0)$ is shown in Fig. 5. In this figure, we display, for spiral wave vector $k_m = k_F$, how the wave functions of the eigenvalues $\pm E$ closest to the Fermi

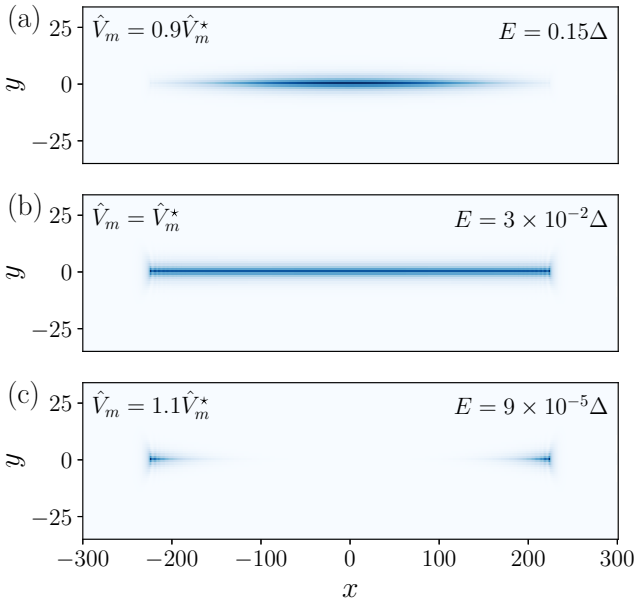


FIG. 5. Real-space map of the absolute square of the wave function for the smallest eigenvalues of a real-space system of 600×70 sites with a spiral magnetic chain extending between sites $x = -224$ to $x = 225$ at $y = 0$, with spiral wave vector $k_m = k_F$. Darker pixels show a larger amplitude; the eigenenergies are $\pm E$ as shown in the panels. The shown amplitudes are summed over spin and particle-hole components and, for better visualization of the end states, we have summed furthermore over both the $+E$ and $-E$ amplitudes. The magnetic impurity potentials \hat{V}_m are chosen to lie (a) below, (b) at, and (c) above the gap closing strength $\hat{V}_m = \hat{V}_m^* = (4t\Delta)^{1/2}$, with t the hopping integral and $\Delta = 0.1t$ the gap function. Panel (c) demonstrates the topological nature of the transition through the appearance of the Majorana end states with energy $E \approx 0$ within the accuracy of the remaining finite-size wave-function overlap.

level change from an extended 1D state to localized end states when \hat{V}_m changes across the gap closing interaction strength \hat{V}_m^* corresponding to C_m^* in the continuum model. For better visualization, we plot the sum of the amplitudes of the two wave functions for $\pm E$. Due to particle-hole symmetry, the amplitudes are the same for the extended states, and for the localized end states, we assure in this way that the states at both ends are visible. We verify furthermore that the values of E (shown as labels in the figure) decrease to $E = 0$ within the numerical accuracy. Only these states are localized and we verified that the other eigenstates remain extended. These end states are thus indeed the particle-hole symmetric Majorana bound states expected from a transition to the topologically nontrivial phase. Through these verifications, we can thus confirm that the topological Hamiltonian $H_{\text{1D}}^{\text{top}}(y = 0)$ indeed produces the correct topological classification.

D. Topology at $y \neq 0$

With the physical significance of the $y = 0$ Hamiltonian verified, we inspect the further y dependence. Since the $H_{\text{1D}}^{\text{top}}(y)$ are a choice, this analysis is principally only qualitative. Nevertheless, we find that the properties underlying the transition from the topology near the chain to the trivial

topology in the bulk are governed by physical and plausible mechanisms. For this reason, we provide a detailed analysis of the y dependence, in particular as it reveals an interesting picture of the extension of the topological regions into space. Furthermore, as we show below, a leading role will be played by the zeros of the Green's function (meaning $\det G = 0$ here), which is otherwise found only for interacting systems [10,11]. Thus the family of 1D Hamiltonians $H_{\text{1D}}^{\text{top}}(y)$ can also be viewed as a simulator of features that otherwise occur only in strongly correlated systems. Here we exhibit these features through the means of $H_{\text{1D}}^{\text{top}}(y)$, but it could similarly be achieved by directly analyzing $G(\omega, k_x, y, y)$ as a class of 1D Green's functions with an effective strong correlation physics whose interaction strength is controlled by y .

We display the topological classification as a function of y in Fig. 6, with $y = 0$ in Fig. 6(a) repeating Fig. 3 for completeness, and with increasing values of $y > 0$ in Figs. 6(b)–6(e). The insets show the corresponding data from the numerical solution of the tight-binding model, repeating Fig. 4 in the inset of Fig. 6(a). At large values of y , the subgap states are all exponentially suppressed and we expect that $H_{\text{1D}}^{\text{top}}(y)$ exhibits only a topologically trivial phase. This is confirmed by Fig. 6(e), which shows that the topological nontrivial region collapses far from the impurity chain. It is interesting to analyze how this collapse occurs, and we observe in Figs. 6(b)–6(e) that it is indeed far from being simple. Most significant is, in Fig. 6(b), the appearance of a second transition line at which for increasing C_m the system again becomes trivial. To understand this behavior, we should notice that the phase diagram of Fig. 6(a) results from the usual crossing of the Fermi level of an eigenvalue of the Hamiltonian.

In terms of the Green's function, a pole then crosses the Fermi level, which coincides with the pole of the T matrix. Since this pole is set by the interaction, it is the same for all y . This is shown by the solid line in all panels in Fig. 6. The only way the sign of the Pfaffian can then change is when a zero of the Green's function instead of a pole crosses the Fermi level, and the zeros of the Green's functions then mark the transitions to the trivial region at large y . In Fig. 6, we have marked the crossing of a zero of the Green's function by a dashed line to distinguish it from the y -independent crossing of the pole shown by the solid line. As y increases, the poles and zeros increasingly coincide, causing the topologically nontrivial region eventually to vanish.

To substantiate these statements, let us look first at the condition $\text{pfaff}[UH_{\text{1D}}^{\text{top}}(y)] = 0$. Since $\det(A) = \text{pfaff}^2(A)$ for any skew symmetric matrix A , this condition is indeed set by the divergence of $\det[G(0, 0, y, y)]$. Such a divergence occurs through the divergence of $\det[T(\omega = 0, k_x = 0)]$, which is precisely the condition for the existence of a subgap state at frequency $\omega = 0$ and momentum $k_x = 0$ used in Part I for the characterization of the subgap spectrum. Since $\omega = 0$, this is the same condition as the gap closure condition at $k_x = 0$, for which we have determined the critical interaction strength C_m^* in Eq. (12). Thus, very close to the interface, the phase transition is governed entirely by the poles of the Green's function.

As y moves away from the interface, the amplitude of the T -matrix term in the Green's function at $\omega = 0$ decays exponentially and $H_{\text{1D}}^{\text{top}}(y) \rightarrow -[g(0, 0, 0)]^{-1}$, which is

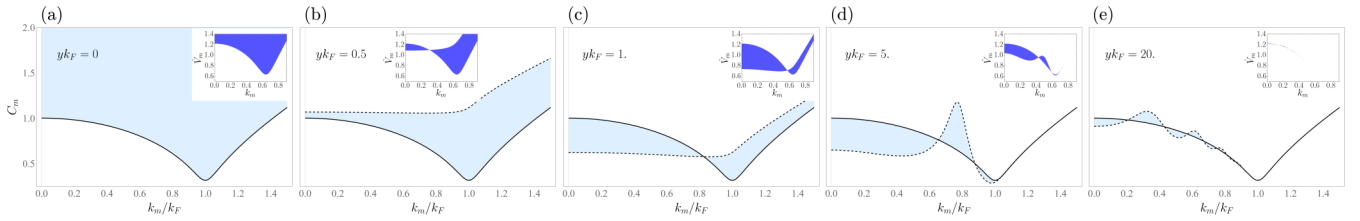


FIG. 6. Topological phase diagrams obtained from the topological Hamiltonians $H_{1D}^{\text{top}}(y)$ as a function of spiral wave number k_m and magnetic scattering strength C_m , for various y and $\tilde{\Delta} = 0.1$. Panel (a) is identical to Fig. 3 and displays the principal phase diagram at $y = 0$. The solid line shows the primary transition at C_m^* [Eq. (12)] between the topologically trivial (white) and nontrivial (blue) regions. Panels (b)–(e) show, with the dashed line, the appearance at $y \neq 0$ of the second transition at strength C_m^{**} [Eq. (30)], determined by the zeros of the Green’s function. At large y , the region spanned between both lines shrinks to zero such that the system becomes trivial throughout. At intermediate distances, oscillations of the dashed line about the solid line show that at the same interaction strength, a region can change topology several times with y , and some trivial regions at $y = 0$ can become nontrivial at some nonzero y . The insets display the corresponding diagrams for the numerical solution of the tight-binding model and show a remarkable correspondence with the continuum model. Differences appear only in the magnitude of regions or are due to limitations of the discrete y values on the lattice as in (b), where there is no lattice site close enough to the interface to directly match $y k_F = 0.5$. The inset of (a) reproduces Fig. 4.

topologically trivial. Since the denominators of G are y independent, the necessary change of sign of the Pfaffian of $H_{1D}^{\text{top}}(y)$ can no longer come from the crossing of a pole of $\det[G(0, 0, y, y)]$. Instead, it has to appear from a pole of $H_{1D}^{\text{top}}(y)$ itself, when one of the eigenvalues diverges, for instance, to $+\infty$ and reappears at $-\infty$. Since $H_{1D}^{\text{top}}(y)$ is given by the inverse Green’s function, the location of this pole corresponds to a zero of $\det[G(0, 0, y, y)]$. In Fig. 7, we visualize this effect by plotting the value of the Pfaffian against magnetic interaction strength C_m for a range of y for $k_m = k_F$. The position of the pole of the Green’s function (at $y \neq 0$) by the square. For increasing y , the pole and zero converge until they overlap and the system remains topologically trivial for all interactions strengths.

The condition $\det[G(0, 0, y, y)] = 0$ actually admits an exact solution for the location of this pole in the Pfaffian. From the exact, full Green’s function defined in Eq. (4), we obtain

$$C_m^{**} = \frac{C_m^*}{\sqrt{1 + e^{-2|y|k_F\delta_-} - 2e^{-|y|k_F\delta_-} \cos(|y|k_F\delta_+)}}}, \quad (30)$$

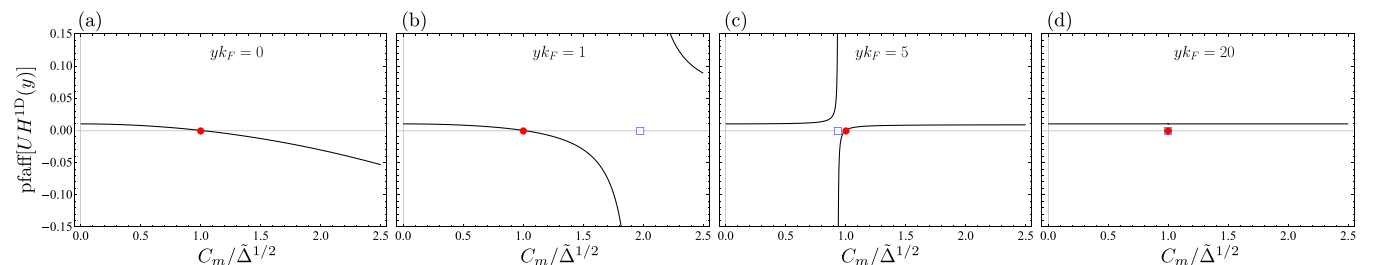


FIG. 7. Pfaffian of the 1D Hamiltonian as a function of magnetic interaction strength C_m for increasing distances y similar to Fig. 6, but for fixed spiral wave number $k_m = k_F$. The interaction strengths are normalized to the critical $C_m = C_m^* = \tilde{\Delta}^{1/2}$ at which the gap closes at $k_x = 0$. The Pfaffian changes its sign at both the zero at $C_m = C_m^*$ (indicated by the red circle) and the pole at $C_m = C_m^{**}$ (blue square) of $H_{1D}^{\text{top}}(y)$. The circle corresponds to the cut through the solid line and the square to the cut through the dashed line in Fig. 6 at $k_m = k_F$. While C_m^* is independent of y , the value of C_m^{**} strongly varies with increasing y . At the large y in (d), the overlap of zero and pole is well seen and the zero eliminates the divergence such that the curve is continuous throughout. This indicates the absence of any topological transition at large distances even at C_m values at which (a)–(c) show the existence of a topologically nontrivial phase nearer the impurity chain.

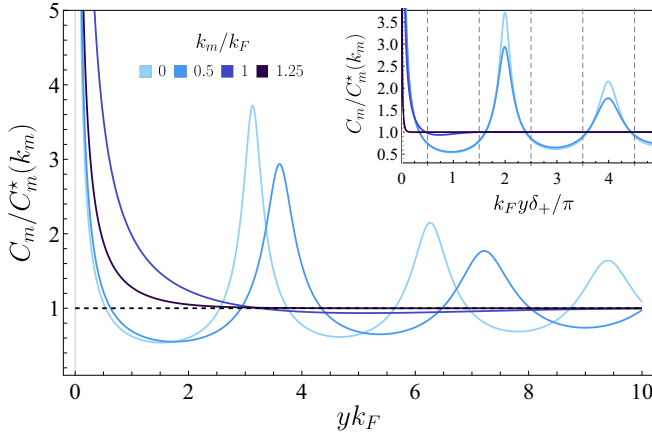


FIG. 8. Plot of the interaction strengths for the zeros $C_m^{**}(y)$ (colored, thick curve) and poles C_m^* (black dashed curve, y independent) of the Green's function as a function of y for a range of spiral wave vectors k_m . The C_m axis is normalized to C_m^* , which depends on k_m . The inset displays the same functions with y normalized to the dimensionless oscillating scale $yk_F\delta_+/\pi$ in Eq. (30). The plots illustrate the generality of the topological strips and the possibility to enter a nontopological phase remotely from the impurity chain (within enclosed regions between the colored, thick curves and black dashed curve).

before settling in the topologically trivial phase. This means that there are strips near the chain that can be considered as alternatively trivial and nontrivial, with a width of the strips set by half of the oscillation scale $\Delta y \sim \pi/k_F\delta_+$. The universality of the latter scale is shown by the inset in Fig. 8. We notice, in particular, that in Fig. 6(c), at $k_m \lesssim 0.8k_F$, entrance to the topological phase is triggered by a zero of the Green's function rather than a pole. This highlights the fact that it is possible for strips at particular $y \neq 0$ to become nontrivial *before* the interface at $y = 0$ itself does as C_m is tuned and without any requirements at all on subgap states. This can be clearly seen in Fig. 8, where there are large regions of space where $C_m^{**} < C_m^*$ and which are thus nontrivial at only a fraction of the magnetic interaction strength required at the interface. Additionally, there can be multiple k_m points [for example, around Fig. 6(d) for $k_m \approx 0.65k_F$ and $\approx 0.87k_F$] where the pole and zero coincide and hence the system is topologically trivial for any magnetic interaction strength C_m .

We should recall here that the topological Hamiltonians $H_{1D}^{\text{top}}(y)$ are only representative for the topological aspects and do not allow a one-to-one matching with physical properties. Nevertheless, they incorporate the natural scales and properties of the system as they are built from the physical Green's function, and as a function of y they have a clear prediction of alternating strips of topologically trivial and nontrivial regions of widths set by the natural scales of the system. Taken as real objects, there would be interfaces between strips of different topological classification and thus suggest the existence of interface states at these interfaces. Since the interfaces are very close together, these interface states all overlap and produce a single wave function with spatial modulation corresponding to the strip widths that is captured by the Green's function. Similar oscillating patterns appear in many other systems from

scattering at any interface or impurity in the form of Friedel-type oscillations. Some examples of oscillating densities and currents in superconductors are found in Refs. [78–83]. Although speculative, it may thus be interesting to see if there could indeed be an interpretation of such oscillating patterns that are found through conventional calculations in terms of the concept of patterns of topologically distinct regions. Such a study is beyond the scope of the present paper.

On the other hand, the Green's function is a physical object that is principally measurable, allowing thus a direct determination of the topological Hamiltonians. The spatial dependence of the subgap states near the magnetic chain can then be used to continuously tune the Hamiltonians and their topology. Each Hamiltonian is then taken as a real object that is simulated by the underlying superconducting system, and the principal topological properties are determined by the zeros of the Green's function as a function of y . As the Green's function at fixed $y = y'$ is a slice out of a higher-dimensional system, it is renormalized by the nontrivial higher-dimensional structure and thus can incorporate structural changes that in a bulk system, would require strong interactions, notably the appearance of its zeros. Through such an interpretation, the discussion of the topological properties given above becomes a reality within the simulated model Hamiltonians.

VI. CONCLUSIONS

In this paper, we investigated the topological properties of the subgap states appearing in a superconductor through scattering on a chain of densely packed magnetic impurities for ferromagnetic or spiral magnetizations. We demonstrated that it is necessary to go beyond a straightforward topological classification attempt. To provide such a classification, the precise form of the Green's function as derived in Part I of this work becomes fundamentally important as it allows one to set up a correct classification method that remains valid for all scattering strengths V_m (or the dimensionless C_m) and all magnetic spiral wave numbers k_m .

We showed how the Green's function provides a precise prescription of the gap closures at $k_x = 0$ and we set up a family of topological Hamiltonians $H_{1D}^{\text{top}}(y)$ that captures, at the position $y = 0$ of the impurity chain, the associated topological phase transitions at any k_m . Through this approach, we circumvented the difficulties we showed to arise from the attempt to extract an effective physical Hamiltonian for the confined subgap states by conventional elimination of the y degree of freedom. It gave us the additional benefit of obtaining a qualitative prescription of how a topologically nontrivial physics near the chain transitions to the topologically trivial regions far from the chain, $y \rightarrow \infty$, where subgap states are absent. This transition is necessarily driven by the zeros of the Green's function, which at large distances align with the singularities and, in this way, neutralize any possible topological phase transition. The oscillations created by the y dependence of the Green's function therefore cause a behavior mimicking the reduction and vanishing of density of states of strongly correlated bulk systems that can also produce a topological phase transition. The y dependence simulates such a behavior and the analysis that is provided shows that it indeed has to

appear in systems of topologically nontrivial states that are confined in some topologically trivial background to guarantee that the bulk topological phase is recovered at large distances.

It should be emphasized though that in this case, the zeros in the Green's function are not a consequence of the spectral function or wave functions becoming zero. One can plot spectral functions through the transition and observe no obvious, sharp change, in contrast to the case of poles of the Green's function where there is a discontinuity. Instead, the zeros are due to a loss of linear dependence in the Green's function caused by competition between the magnetic interaction strength and the background superconductor. This results in an emergent symmetry between states, expressed by the alignment of a zero with a pole with increasing y , which can be compared to transitions governed by poles where states move in frequency space and, by careful tuning, can coincide with high symmetry points in configuration space. This property thus assures the fitness of these Hamiltonians for the spatially dependent topological classification.

Interestingly, the spatial oscillations of the subgap wave functions can lead to the appearance of multiple strips of different topological index in the vicinity of the chain. This may be compared with layers of different materials, but due to the constructed nature of the topological Hamiltonians, any physical implications would remain speculative. In addition, these layers are very narrow, below the superconducting coherence length and Fermi wavelength, so that any features that could arise from interfacing different materials would be washed out broadly through many layers. Yet there are situations in which the topology near the impurity chain is trivial and a nontrivial strip appears only at a distance. This raises the general question as to whether it could be possible to design spatial patterns of regions with different topological properties by interference of such wave functions arising from an astute placement of magnetic scatterers.

The work presented in this paper is theoretical. No data were produced, and supporting research data are not required.

ACKNOWLEDGMENTS

We thank T. Cren, R. Queiroz, T. Ojanen, C. Hooley, and P. Simon for stimulating discussions, and A. V. Balatsky for discussions during the early stage of this work. C.J.F.C. acknowledges studentship funding from EPSRC under Grant No. EP/M506631/1.

APPENDIX: SUBGAP BANDS FROM SELF-CONSISTENT NUMERICS

We employ the tight-binding model introduced in Part I for comparison with the analytical model and validation of the results. This model is defined through the Hamiltonian

$$H = - \sum_{\langle i,j \rangle, \sigma} t c_{i,\sigma}^\dagger c_{j,\sigma} - \sum_{i,\sigma} \mu c_{i,\sigma}^\dagger c_{i,\sigma} + \sum_i [\Delta_i c_{i,\downarrow} c_{i,\uparrow} + \text{H.c.}] \quad (\text{A1})$$

The indices i, j run over the sites of a 2D square lattice of size $N_x \times N_y$ with periodic boundary conditions, and $\langle i, j \rangle$ denotes the restriction to nearest neighbors. We write $i = (i_x, i_y)$ to access the 2D coordinates of site i . The hopping integral is t , the pairing amplitude Δ , and the chemical potential μ . The operators $c_{i,\sigma}$ annihilate an electron of spin σ on site i , and $c_{i,\sigma}^\dagger$ are the corresponding creation operators.

The interactions with the magnetic impurities have amplitudes \hat{V}_m (denoted differently from the V_m of the continuum model) and are expressed through the Hamiltonian

$$H_m = \hat{V}_m \sum_{i=(i_x,0)} \mathbf{M}_i \cdot \mathbf{S}_i. \quad (\text{A2})$$

Here, $\mathbf{S}_i = \sum_{\sigma,\sigma'} \sigma_{\sigma,\sigma'} c_{i,\sigma}^\dagger c_{i,\sigma'}$ are the electron spin operator, for σ the vector of Pauli matrices, and \mathbf{M}_i are unit vectors that are either aligned ferromagnetically or wind in a planar spiral with wave number k_m in the spin (x, y) plane.

For the finite chain in Fig. 5, we consider a system of size $N_x = 600, N_y = 70$ and restrict H_m to values $-224 \leq i_x \leq 225$ at $i_y = 0$. The parameters are chosen such that $\Delta = 0.1t$, $\mu = -3.6t$, and $ak_F = \arccos[(-\mu - 2t)/(2t)] \approx 0.64$.

For the chains with infinite x extension, we partially diagonalize the Hamiltonian by performing the Fourier transform $i_x \rightarrow k_x$. For a ferromagnetic alignment ($k_m = 0$), this is done directly. For spiral magnetizations with k_m , we choose the spin axes such that \mathbf{M}_i rotates in the spin- (x, y) plane so that the same gauge transformation $k_x \rightarrow k_x \pm k_m$ as for the continuum model maps the spiral back to a ferromagnetic alignment. The periodic boundary conditions along the x directions are always applied in the gauge-transformed basis. Solutions are carried out as described further in Part I.

Green's functions are obtained through the Lehmann representation in terms of the eigenfunctions and eigenvalues of the Hamiltonian, as a function of k_x, i_y, i'_y , and ω . Topological invariants are calculated by self-consistent determination of the full Hamiltonian, followed by the calculation of the Pfaffian invariant of the 1D topological Hamiltonians obtained from the inverse of the Green's function at $i_y = i'_y, k_x = 0$, and $\omega = 0$ in the same way as for the analytic model described in Sec. V. We include only the single time-reversal invariant momentum $k_x = 0$ rather than adding the influence of the $k_x = \pi/a$ point for better comparison to the continuum model.

In Fig. 4 as well as in the insets of Fig. 6, the system size is $N_x = 51$ and $N_y = 100$, and the gap is self-consistently tuned to $\Delta = 0.1t$ for $\hat{V}_m = 0$. The self-consistent parameters so determined are then used as input to the diagonalization of the Hamiltonian with added magnetic impurity chain with a variety of \hat{V}_m and k_m values to determine the phase diagrams. The insets correspond to phase diagrams at sites (a) $i_y = 50$ (i.e., the center), (b) $i_y = 51$, (c) $i_y = 52$, (d) $i_y = 58$, and (e) $i_y = 81$. As $ak_F \approx 0.64$, these roughly correspond to the values for yk_F displayed for the continuum phase diagrams. Note that due to the numerics being on a lattice, (b) is as close to the interface as possible but is not sufficiently close to exactly match the behavior seen in the continuum model.

- [1] C.-K. Chiu, J. C. Y. Teo, A. P. Schnyder, and S. Ryu, *Rev. Mod. Phys.* **88**, 035005 (2016).
- [2] J. K. Pachos, *Introduction to Topological Quantum Computation* (Cambridge University Press, Cambridge, 2012).
- [3] A. P. Schnyder, S. Ryu, A. Furusaki, and A. W. W. Ludwig, *Phys. Rev. B* **78**, 195125 (2008).
- [4] A. P. Schnyder, S. Ryu, A. Furusaki, and A. W. W. Ludwig, in *Advances in Theoretical Physics: Landau Memorial Conference*, edited by V. Lebedev and M. Feigel'man, AIP Conf. Proc. No. 1134 (AIP, New York, 2009), p. 10.
- [5] A. Kitaev, in *Advances in Theoretical Physics: Landau Memorial Conference*, edited by V. Lebedev and M. Feigel'man, AIP Conf. Proc. No. 1134 (AIP, New York, 2009), p. 22.
- [6] S. Ryu, A. P. Schnyder, A. Furusaki, and A. W. W. Ludwig, *New J. Phys.* **12**, 065010 (2010).
- [7] Z.-C. Gu and X.-G. Wen, *Phys. Rev. B* **80**, 155131 (2009).
- [8] X. Chen, Z.-C. Gu, Z.-X. Liu, and X.-G. Wen, *Phys. Rev. B* **87**, 155114 (2013).
- [9] L. Fidkowski and A. Kitaev, *Phys. Rev. B* **83**, 075103 (2011).
- [10] G. Volovik, *The Universe in a Helium Droplet* (Oxford University Press, Clarendon Press, 2003).
- [11] V. Gurarie, *Phys. Rev. B* **83**, 085426 (2011).
- [12] Z. Wang and S.-C. Zhang, *Phys. Rev. X* **2**, 031008 (2012).
- [13] Z. Wang, X.-L. Qi, and S.-C. Zhang, *Phys. Rev. B* **85**, 165126 (2012).
- [14] Z. Wang and S.-C. Zhang, *Phys. Rev. B* **86**, 165116 (2012).
- [15] Z. Wang and B. Yan, *J. Phys.: Condens. Matter* **25**, 155601 (2013).
- [16] S. Rachel, *Rep. Prog. Phys.* **81**, 116501 (2018).
- [17] C. J. F. Carroll and B. Braunecker, *Phys. Rev. B* **104**, 245133 (2021).
- [18] M.-D. Choi, *Linear Algebra Appl.* **10**, 285 (1975).
- [19] W. F. Stinespring, *Proc. Am. Math. Soc.* **6**, 211 (1955).
- [20] G. C. Ménard, S. Guissart, C. Brun, S. Pons, V. S. Stolyarov, F. Debontridder, M. V. Leclerc, E. Janod, L. Cario, D. Roditchev, P. Simon, and T. Cren, *Nat. Phys.* **11**, 1013 (2015).
- [21] G. C. Ménard, S. Guissart, C. Brun, M. Trif, F. Debontridder, R. T. Leriche, D. Demaille, D. Roditchev, P. Simon, and T. Cren, *Nat. Commun.* **8**, 2040 (2017).
- [22] T. P. Choy, J. M. Edge, A. R. Akhmerov, and C. W. J. Beenakker, *Phys. Rev. B* **84**, 195442 (2011).
- [23] M. Kjaergaard, K. Wölms, and K. Flensberg, *Phys. Rev. B* **85**, 020503(R) (2012).
- [24] S. Nadj-Perge, I. K. Drozdov, B. A. Bernevig, and A. Yazdani, *Phys. Rev. B* **88**, 020407(R) (2013).
- [25] F. Pientka, L. I. Glazman, and F. von Oppen, *Phys. Rev. B* **88**, 155420 (2013).
- [26] F. Pientka, L. I. Glazman, and F. von Oppen, *Phys. Rev. B* **89**, 180505(R) (2014).
- [27] K. Pöyhönen, A. Westström, J. Röntynen, and T. Ojanen, *Phys. Rev. B* **89**, 115109 (2014).
- [28] J. Röntynen and T. Ojanen, *Phys. Rev. B* **90**, 180503(R) (2014).
- [29] Y. Kim, M. Cheng, B. Bauer, R. M. Lutchyn, and S. Das Sarma, *Phys. Rev. B* **90**, 060401(R) (2014).
- [30] A. Heimes, P. Kotetes, and G. Schön, *Phys. Rev. B* **90**, 060507(R) (2014).
- [31] N. Y. Yao, L. I. Glazman, E. A. Demler, M. D. Lukin, and J. D. Sau, *Phys. Rev. Lett.* **113**, 087202 (2014).
- [32] I. Reis, D. J. J. Marchand, and M. Franz, *Phys. Rev. B* **90**, 085124 (2014).
- [33] A. Heimes, D. Mendler, and P. Kotetes, *New J. Phys.* **17**, 023051 (2015).
- [34] A. Westström, K. Pöyhönen, and T. Ojanen, *Phys. Rev. B* **91**, 064502 (2015).
- [35] P. M. R. Brydon, S. Das Sarma, H.-Y. Hui, and J. D. Sau, *Phys. Rev. B* **91**, 064505 (2015).
- [36] M. Schechter, M. S. Rudner, and K. Flensberg, *Phys. Rev. Lett.* **114**, 247205 (2015).
- [37] W. Hu, R. T. Scalettar, and R. R. P. Singh, *Phys. Rev. B* **92**, 115133 (2015).
- [38] M. H. Christensen, M. Schechter, K. Flensberg, B. M. Andersen, and J. Paaske, *Phys. Rev. B* **94**, 144509 (2016).
- [39] M. Schechter, K. Flensberg, M. H. Christensen, B. M. Andersen, and J. Paaske, *Phys. Rev. B* **93**, 140503(R) (2016).
- [40] K. Pöyhönen, A. Westström, and T. Ojanen, *Phys. Rev. B* **93**, 014517 (2016).
- [41] B. Braunecker and P. Simon, *Phys. Rev. Lett.* **111**, 147202 (2013).
- [42] J. Klinovaja, P. Stano, A. Yazdani, and D. Loss, *Phys. Rev. Lett.* **111**, 186805 (2013).
- [43] M. M. Vazifeh and M. Franz, *Phys. Rev. Lett.* **111**, 206802 (2013).
- [44] B. Braunecker and P. Simon, *Phys. Rev. B* **92**, 241410(R) (2015).
- [45] Y. Peng, F. Pientka, L. I. Glazman, and F. von Oppen, *Phys. Rev. Lett.* **114**, 106801 (2015).
- [46] S. Hoffman, J. Klinovaja, and D. Loss, *Phys. Rev. B* **93**, 165418 (2016).
- [47] L. Yu, *Acta Phys. Sin.* **21**, 75 (1965).
- [48] H. Shiba, *Prog. Theor. Phys.* **40**, 435 (1968).
- [49] A. I. Rusinov, *JETP Lett.* **9**, 85 (1969).
- [50] C.-H. Hsu, P. Stano, J. Klinovaja, and D. Loss, *Phys. Rev. B* **92**, 235435 (2015).
- [51] B. Braunecker, P. Simon, and D. Loss, *Phys. Rev. Lett.* **102**, 116403 (2009).
- [52] B. Braunecker, P. Simon, and D. Loss, *Phys. Rev. B* **80**, 165119 (2009).
- [53] B. Braunecker, G. I. Japaridze, J. Klinovaja, and D. Loss, *Phys. Rev. B* **82**, 045127 (2010).
- [54] A. Y. Kitaev, *Phys. Usp.* **44**, 131 (2001).
- [55] C. L. Kane and E. J. Mele, *Phys. Rev. Lett.* **95**, 146802 (2005).
- [56] L. Fu and C. L. Kane, *Phys. Rev. B* **74**, 195312 (2006).
- [57] T. D. Stanescu, R. M. Lutchyn and S. Das Sarma, *Phys. Rev. B* **84**, 144522 (2011).
- [58] D. J. Thouless, M. Kohmoto, M. P. Nightingale, and M. den Nijs, *Phys. Rev. Lett.* **49**, 405 (1982).
- [59] J. Zak, *Phys. Rev. Lett.* **62**, 2747 (1989).
- [60] Z. Wang, X.-L. Qi, and S.-C. Zhang, *Phys. Rev. Lett.* **105**, 256803 (2010).
- [61] J. C. Budich and B. Trauzettel, *Phys. Status Solidi RRL* **7**, 109 (2013).
- [62] A. Westström, K. Pöyhönen, and T. Ojanen, *Phys. Rev. B* **94**, 104519 (2016).
- [63] Y.-M. Xie, K. T. Law, and P. A. Lee, *Phys. Rev. Res.* **3**, 043086 (2021).
- [64] J. D. Sau, R. M. Lutchyn, S. Tewari, and S. Das Sarma, *Phys. Rev. Lett.* **104**, 040502 (2010).
- [65] Y. Oreg, G. Refael, and F. von Oppen, *Phys. Rev. Lett.* **105**, 177002 (2010).

- [66] R. M. Lutchyn, J. D. Sau, and S. Das Sarma, *Phys. Rev. Lett.* **105**, 077001 (2010).
- [67] K. Kraus, *Ann. Phys.* **64**, 311 (1971).
- [68] D. Asahi and N. Nagaosa, *Phys. Rev. B* **86**, 100504(R) (2012).
- [69] P. Beck, L. Schneider, L. Rózsa, K. Palotás, A. Lászlóffy, L. Szunyogh, J. Wiebe, and R. Wiesendanger, *Nat. Commun.* **12**, 2040 (2021).
- [70] N. Sedlmayr, V. Kaladzhyan, and C. Bena, *Phys. Rev. B* **104**, 024508 (2021).
- [71] C. J. Carroll, Designed topological states from hybrid spiral magnet-superconductor heterostructures, Ph.D. thesis, University of St. Andrews, 2019.
- [72] R. Bianco and R. Resta, *Phys. Rev. B* **84**, 241106(R) (2011).
- [73] M. B. Hastings and T. A. Loring, *Ann. Phys.* **326**, 1699 (2011).
- [74] E. Prodan, T. L. Hughes, and B. A. Bernevig, *Phys. Rev. Lett.* **105**, 115501 (2010).
- [75] E. Prodan, *J. Phys. A: Math. Theor.* **44**, 113001 (2011).
- [76] E. Mascot, S. Cocklin, S. Rachel, and D. K. Morr, *Phys. Rev. B* **100**, 184510 (2019).
- [77] E. Mascot, C. Agrahar, S. Rachel, and D. K. Morr, *Phys. Rev. B* **100**, 235102 (2019).
- [78] M. Matsumoto and M. Sgrist, *J. Phys. Soc. Jpn.* **68**, 994 (1999).
- [79] Q. H. Wang and Z. D. Wang, *Phys. Rev. B* **69**, 092502 (2004).
- [80] B. Horovitz and A. Golub, *Phys. Rev. B* **68**, 214503 (2003).
- [81] B. Braunecker, P. A. Lee, and Z. Wang, *Phys. Rev. Lett.* **95**, 017004 (2005).
- [82] Y. E. Kraus, A. Auerbach, H. A. Fertig, and S. H. Simon, *Phys. Rev. Lett.* **101**, 267002 (2008).
- [83] L. Lauke, M. S. Scheurer, A. Poenicke, and J. Schmalian, *Phys. Rev. B* **98**, 134502 (2018).